Atmospheric visibility inferred from continuous-wave Doppler wind lidar

Manuel Queißer[1], Michael Harris[1], Steven Knoop[2]

5   [1] ZX Lidars, The Old Barns, Fairoaks Farm, Hollybush, Ledbury, HR8 1EU, U.K.

[2] Royal Netherlands Meteorological Institute (KNMI), Utrechtseweg 297, 3731 GA, De Bilt, the Netherlands

Correspondence to: Manuel Queißer (manuelqueisser@web.de)

Abstract. Atmospheric visibility, or meteorological optical range (MOR), is governed by light extinction by aerosols. State-of-the-art visibility sensors, such as employed in meteorological observatories and airports, infer MOR by either measuring

10   transmittance or scattering. While these sensors yield robust measurements with reasonable accuracy (10% to 20%), they measure in situ. MOR from these sensors may thus not be representative of MOR further away, for example, under conditions with stratified aerosol types. This includes off-shore sites near the sea surface during conditions with advection fog, sea spray or mist. Elastic backscatter lidar can be used to measure light extinction and has previously demonstrated to be a powerful method to infer visibility. Lidar can measure visibility not just near the instrument, but further away (remotely) and single-

15   ended, whilst capable of measuring profiles of MOR along atmospheric slant paths. Continuous-wave (CW) Doppler wind lidar systems make up one of the most widespread type of elastic backscatter lidar and are typically used in wind resource assessment. Using these existing platforms for remote and single-ended measurement of MOR-profiles could allow for new and valuable applications. However, the low light extinction associated with this type of lidar excludes the use of the extinction coefficient for MOR retrieval, but leaves the backscatter coefficient as a possible proxy for MOR, though with an accuracy

20   expected to be inferior to the former method. We analysed backscatter data from CW wind lidar and co-measured MOR from visibility sensors from two campaigns (Cabauw, Netherlands and Pershore, United Kingdom) and found backscatter from CW wind lidar to be a viable proxy of MOR if calibrated against a visibility sensor. The expected accuracy of the method is low and of order of few kilometres. This means MOR from CW wind lidar could be used in safety uncritical problems, such as assessment of visibility of man-made objects, including wind turbines. The high sensitivity of the lidar backscatter to aerosol

25   type and size distribution could open up additional applications, such as volcanic plume monitoring.

1 Introduction

Visibility is how well we can see something. More specifically, atmospheric visibility is the maximum horizontal distance an object can be seen through the atmosphere with the naked eye. Visibility is traditionally estimated doing exactly that, namely by measuring the maximum distance a dark object with a suitable size can be seen on the horizon against the surrounding sky.

30   The visibility of a distant object is a function of several factors, including the object's colour, the angle of the sun and Earth's curvature. However, at constant illumination by the sun, the governing physical mechanism of visibility is the extinction of light by scattering through aerosols suspended in the atmosphere. This leads to the definition of meteorological optical range (MOR), which quantifies that part of visibility that is caused by light extinction. The MOR therefore provides a quantifiable estimate of atmospheric visibility. The world meteorological organization defines MOR as the length of path in the atmosphere

35   required to reduce the luminous flux in a collimated beam from an incandescent lamp, at a color temperature of 2700 K, to 5 per cent of its original value, the luminous flux being evaluated by means of the photometric luminosity function of the International Commission on Illumination (Jones et al., 1990). Note that a blackbody temperature of 2700 K corresponds to about 1100 nm. For daylight conditions, MOR is commonly defined as the horizontal range for which the light intensity contrast between the object and the surrounding sky is either C_t=2%, or, as later suggested, 5% (Middleton 1947, Dabberdt

40   and Eigsti 1981; Nebuloni, 2005). Adopting the well-known Bouguer–Lambert–Beer law and C_t=5%, MOR can be written as

$$MOR = \frac{-\ln(C_t)}{\sigma} \approx \frac{3}{\sigma}, \quad\quad\quad (1)$$

where σ is the atmospheric extinction coefficient (in units of m^{-1}). Hence, by measuring the light extinction σ, MOR can be derived. In practice, MOR is evaluated at a wavelength of 550 nm, close to the human eye's sensitivity maximum (Nebuloni,

45   2005). In the rest of the paper the terms visibility and MOR are used interchangeably.

        The traditional method of estimating MOR using human visual observation of targets of well-defined distance and albedo delivers values reasonably close to MOR from Eq. (1) and has the advantage that the visibility does not need to be translated into a quantity perceptible to humans. The WMO recommends to measure visibility at a height ca. 2 m above ground, close to human line of sight (Jones et al., 1990).

50   This is also the height at which state of the art visibility sensors, or visiometers, determine MOR. These visiometers either measure atmospheric transmittance along an optical path of fixed distance or the intensity of forward scattered light, from which the extinction coefficient can be retrieved (Crosby, 2003; Werner et al. 2005). One main difference between these two approaches is that unlike the transmissivity metre, a sensor measuring forward scattering needs a very small optical path only (~10 cm), i.e. it measures in situ, which makes alignment and maintenance easy. Arguably, this risks to sample a portion

55   of the sky that is not representative of the wider atmospheric conditions. Both of these approaches are bound to measure visibility at the height they are mounted at, usually few metres above ground level (agl) and both are double-ended, meaning the receiver is located at the opposite end of the optical transmitter.

        The aerosol number density, and thus the visibility, is generally a function of height agl. Especially offshore, a strong vertical stratification at the sea/atmosphere interface due to condensation caused by advection is to be expected. A visibility

60   sensor mounted a few metres above the sea surface (e.g. at the beach or on a buoy) could be immersed in a layer of spray or haze, giving a biased visibility reading. An effective visibility measured vertically, rather than horizontally, considering aerosol stratification effects in the boundary layer, or, more generally, a slant optical range (SOR, Werner et al., 2005) may be more desirable for some applications (Fig.1). For large features, such as mountains or man-made structures exceeding 100 m height,

65 it may be more beneficial to measure an effective visibility at or near the actual line of sight between the observer's eye and the feature, which would be significantly higher above ground than only a few metres. For example, the height at half distance for a 100 m high object located 10 km away from the observer would be ~50 m agl.

Figure 1. Visibility of wind turbines offshore. The wind turbines are forming an optical contrast against a clear sky with moderate mist near the sea surface, which reduces visibility for the lower parts of the wind turbines. Photo from: SSE Renewables.

70   Light detection and ranging (lidar) allows a spatially integrated measurement of atmospheric visibility, in a single ended manner and remotely, with ranges of hundreds to kilometres away from the lidar. MOR measured with pulsed elastic backscatter lidar, including ceilometers, has shown good agreement with standard in-situ sensors, such as transmissometer and visibility sensors (Werner et al., 2005; Pantazis et al., 2017; Hongda et al., 2017; Hu et al., 2021). Shang et al. (2017) compared visibility from a pulsed backscatter lidar with visibility from a visibility sensor and found excellent agreement. Lidar is ideal

75 for atmospheric sounding, which means it is able to measure visibility not only at a single location remotely, but at several points along the lidar line of sight, yielding a visibility profile. The return power of pulsed backscatter lidar is a function of both the backscatter coefficient and the atmospheric extinction coefficient. Therefore, the lidar return signal contains information about the atmospheric extinction and hence the visibility. The retrieval of the visibility is based on solving the lidar equation for both the atmospheric extinction coefficient and the backscatter coefficient. Retrieval techniques include

80 inversion (e.g. Werner et al., 2005) and iterative measurements starting from an aerosol free reference height (Pantazis et al., 2017).

        Single-ended retrieval of visibility inferred from the backscatter coefficient only has successfully been demonstrated too (Curcio et al., 1958; Vogt 1968), but, as opposed to lidar, by using polychromatic light. The backscatter coefficient has a higher sensitivity to the size of the aerosols along the beam path and hence to the aerosol size distribution (SD) than the

85 extinction coefficient. These fluctuations are smoothed considerably when the emitted photons are polychromatic, leading to accuracies of the order of 20% (Twomey and Howell, 1965), which is comparable to forward scattering visiometers (Biral

SWS Series user manual, 2017; Cambell Scientific CS125 user manual, 2016; Crosby, 2003). Vogt (1968) found that the backscatter coefficient is useful to infer visibility, but it needs to be calibrated against a visibility sensor in an atmosphere similar (similar mean aerosol SD) to the one of its intended use. Monochromatic light, as commonly used in lidar, was found to yield a poorer, more scattered correlation between backscattered light intensity and visibility, with an associated scattering around 50% of backscattered intensity for a given visibility (Twomey and Howell, 1965).

Amplitude modulated direct detection continuous wave (CW) lidar has also been proposed and demonstrated to measure MOR by relating it to the phase shift between transmitted and received photons (Schappert 1971; Kreid 1976; Button, 1977). Provided a homogenous atmosphere, the phase shift depends on the extinction coefficient, avoiding the dependence on the backscatter coefficient (Kreid 1976).

Coherent CW Doppler wind lidar has not been used yet to measure visibility. Thousands of these lidars are being deployed worldwide, especially in wind resource assessment campaigns (Emeis et al., 2007). Coherent CW wind lidars are designed to measure wind field quantities such as speed, direction and turbulence index at heights between tens and few hundreds of metres. Similar to other backscatter lidar systems, a CW Doppler wind lidar measures the light power returned from atmospheric aerosols moving with the wind stream lines. Therefore, CW wind lidar is in principle able to measure visibility, in particular SOR, single-ended and remotely and at different heights (profiling). However, the influence of atmospheric extinction scales with measurement range and wavelength (light with longer wavelength is scattered less). Due to the longer wavelength (~1550 nm) of most CW wind lidars compared with visible backscatter lidars described above, at normal working ranges (up to 300 m), the return signal is not sensitive to atmospheric extinction, but is practically governed by the backscatter coefficient only. This leaves the backscatter coefficient (henceforth termed backscatter) as the most obvious proxy of visibility of a CW wind lidar.

The aforementioned studies do suggest a correlation between visibility and backscatter, but at relatively poor accuracy, since CW wind lidar is inherently monochromatic. The accuracy may, however, suffice for non-safety critical applications, such as estimates of minimum or maximum visibility. An example would be the visibility of manmade structures such as wind turbines, towers or bridges. A relation between signal strength of CW wind lidar and visibility is evident from everyday operation, but has not been quantified yet. Thousands of wind lidar systems already in operation worldwide could be used to yield a useful remote measure of visibility add no extra cost. This could open new applications of these existing systems in commercial or scientific applications. Systems used for scientific or observational use could provide for a denser, more global data set of visibility. In the present case study, we use datasets from two different measurement campaigns, in Cabauw (Netherlands) and Pershore (UK), to assess if backscatter from CW wind lidar can be used to retrieve meaningful estimates of visibility. The wind lidar used in both campaigns and the visibility sensors are briefly detailed. After that, two methods to retrieve visibility from backscatter are described. Results from the two methods are presented thereafter and discussed before conclusions are drawn.

2 Method and Material

2.1 CW wind lidar operating principles

Both vertical profiling wind lidars used in the two measurement campaigns are of type ZX 300 (ZX Lidars, UK, formerly ZephIR Lidar). An overview of some of the properties and settings of the ZX 300 as deployed at Cabauw is given in Table 1. The ZX 300 is a homodyne coherent detection CW focusing wind lidar. The laser beam is transmitted through a constantly rotating prism (wedge) to perform a so-called velocity azimuth display (VAD) scan with a scanning cone angle of ~30˚ (with respect to zenith). Up to 10 measurement heights can be configured, in addition to a pre-fixed height of 39 m agl, which are permuted through in descending order. Once a measurement height is set by focusing the laser beam, the focus performs a circular scan for 1-second, split into 50 points with ~20 ms integration time, separated by 360/50˚. The 50 measurements are used to reconstruct the vertical and horizontal wind speed components. The optimum height range is 10–200 m above the instrument, although higher heights can be set in the software. By virtue of the geometrical focusing, the probe length increases quadratically with measurement distance (height): at 10 m height above the instrument, the -3dB probe length is 0.07 m, whereas at 200 m it is 30 m. CW focusing wind lidars can be sensitive to clouds that are above the maximum range, as the contribution to the Doppler signal from clouds in the tail of the laser pulse profile can be comparable to the aerosol signal at the preselected focusing height (Smith et al., 2006). A cloud removal algorithm is used to correct for this effect, which involves a measurement at an additional higher altitude. For a CW coherent wind lidar, such as the ZX 300, the time-averaged optical signal power P_S backscattered by aerosols into the receiving telescope is given to a good approximation by (Harris et al., 2001)

$$P_S = \pi P_T \beta(\pi) \lambda, \tag{2}$$

where P_T is the transmitted laser power and $\beta(\pi)$ is the atmospheric backscatter coefficient, and λ is the laser wavelength. Note that Eq. (2) contains no dependence on either the focus range or the system aperture size. With a typical value of 10^{-8} m^{-1} sr^{-1} for $\beta(\pi)$ in relatively clear boundary layer air a transmitted power P$_T$ of typically ~1 W and λ ~1.5 μm, the received power P_S derived from Equation (2) is of order 5×10^{-14} W (50 femtowatts) only. Assuming shot noise limited detection, the carrier-to-noise-ratio of a coherent CW lidar is given by (Harris et al., 2001)

$$CNR = \frac{\eta P_S}{\frac{hc}{\lambda}\Delta v[1+D(v)]}, \tag{3}$$

where η is the quantum efficiency of the detector, h is Planck's constant, c the speed of light, Δv the coherent detection bandwidth and $D(v)$ is the detector dark noise spectral density. Combining Eqns. (2) and (3) yields the relationship used to retrieve the backscatter coefficient:

$$\beta(\pi) = \frac{\left(\frac{hc}{\lambda}\right)\Delta v \,[1+D(v)]NB}{\pi\eta\lambda P_t} \equiv Z\,B, \tag{4}$$

with $CNR \equiv NB$, where N is the number of bins of the discrete Doppler spectrum of the lidar, B is the average heterodyne signal power spectral density per bin and computed as

$$B = \frac{1}{N}\sum_{i=0}^{N-1} P_i \,, \tag{5}$$

where P_i is the power spectral density of bin i. Plugging in numbers typical for a ZX 300 yields $Z = 1.3 \times 10^{-6}$ m^{-1} sr^{-1}, which is a constant for a given transmitted optical power. If not written otherwise, backscatter values are henceforth written as $\beta(\pi)/Z$.

Table 1. Key parameters of a ZX 300 wind lidar. The measurement heights are specific to the Cabauw site, all other parameters are generic.

Laser wavelength	1560 nm
Optical laser power	1.3 W
Ranging	Geometric focusing
Horizontal wind retrieval	VAD scan
Measuring heights	11, 20, 39, 80, 140, 200, 252 m agl
Scan dwell time	1 s
Height instrument	1 m

2.2 Description of data and field site

Data from a visibility sensor and from the wind lidar are retrieved for two sites: Cabauw, Netherlands and the UK remote sensing test site in Pershore, UK.

The UK remote sensing test facility at Pershore is located in a flat, rural setting at a former airbase (52.143° N, 2.037° W, Fig. 2a). The Pershore data set covers 24 months, from 1/1/2018 to 1/1/2020. A single visibility sensor of type Campbell Scientific 120/125 was available at Pershore, mounted at 2 m agl on a mast on a meteorological measurement site operated by the UK Met Office, located ~600 m away from the lidar (Fig. 2b). The Campbell Scientific 120/125 uses a 42˚ scatter angle (Cambell Scientific CS125 user manual). The measurement accuracy is ±10% (visibility up to 10 km), ±15% (visibility up to 15 km) and ±20% for visibilities above 15 km.

The Cabauw Experimental Site for Atmospheric Research (CESAR) is located in an extended and flat polder landscape, about 40 km off the coast, 0.7 m below mean sea level (51.971˚ N, 4.927˚ E; Fig. 2a), run by the Royal Netherlands Meteorological Institute (KNMI) and is part of the Ruisdael Observatory. The visibility data used were acquired during a wind measurement campaign described in detail in Knoop et al. (2021) and their measurement is part of a regular observation program (Bosveld, 2020). The coinciding data from the wind lidar and the visibility sensors for Cabauw used here cover about 24 months, from 15/2/2018 to 29/2/2020. The visibility was measured with visiometers of type Biral SWS100 at heights agl of 10 m and 20 m at a meteorological mast called mast B, and at 40 m, 80 m, 140 m and 200 m at mast A (depicted in Fig. 2c). The visiometers measure the forward scattered intensity at 45˚ (Biral SWS100 user manual). The accuracy of the visibilities as reported in the user manual are between ±10% (up to 16 km) and ±20 km (16 km to 30 km). The relevant measurement heights agl of the wind lidar were 11 m, 20 m, 39 m, 80 m, 100 m, 140 m and 200 m (Table 1). The ZX 300 wind lidar was

located 293 m away from mast A and 267 m away from mast B (Fig. 2b). Due to the extended probe length of the lidar, height mismatches of 1 m between lidar measurement height and sensor height are expected to be insignificant.

Both visiometer types at Cabauw and Pershore use the same principle of operation, so that the differences between the two types of visiometers are expected to be much smaller than between visiometer and wind lidar. All data from the
180   visibility sensors are time series with visibility in units of metres. As stated above, the backscatter coefficients from the wind lidars are time series in units of 1.3×10^{-6} m^{-1} sr^{-1}. Both wind and visibility data are averaged over 10 min long periods.
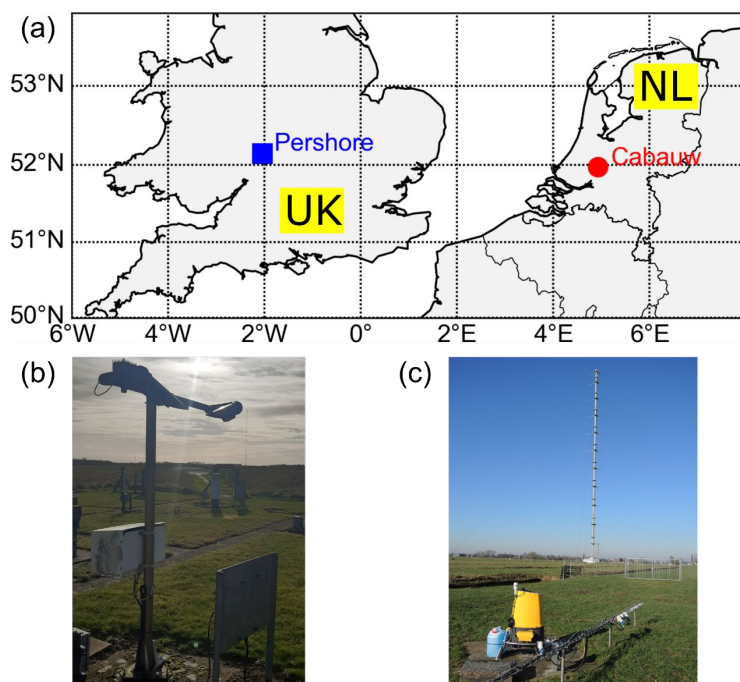
Figure 2. Location of lidar and visibility sensors (visiometers). (a) Pershore (United Kingdom, UK) and Cabauw (Netherlands, NL). (b) Visiometer at Pershore with meteorological mast in the background where the wind lidar is located. (c) ZX 300 wind lidar at
185   **Cabauw with meteorological mast A in the background.**

2.3 Retrieval of visibility from the backscatter coefficient

2.3.1 Method A: Directly converting backscatter to visibility

The retrieved backscatter coefficients from Eq. (4) are directly related to visibility as follows. The ratio between the extinction
190   and the backscatter coefficient, the extinction-to-backscatter ratio (also called lidar ratio) S is used to estimate the extinction coefficient from the backscatter coefficient as (Doherty et al., 1999)

$$\sigma = \beta(\pi)S, \hspace{4cm} (6)$$

where $\beta(\pi)$ is the backscatter coefficient. S is assumed to be constant (Young and Vaughan, 2009). However, S can vary for common atmospheric aerosols from 1 to about 100 sr, depending on the SD, shape, and chemical composition of the particles

195   (Fernald et al., 1972; Doherty et al., 1999), as will be discussed further below. The empirical power law by Ångström is used

to relate the extinction coefficient measured at the lidar wavelength of ~1550 nm to 550 nm (Nebuloni, 2005; Schuster et al.,

2006; Shang et al., 2017) as

$$\sigma_0 = \sigma_1 \left(\frac{\lambda_1}{\lambda_0}\right)^\alpha, \qquad (7)$$

where α is the Ångström coefficient, λ_0 and λ_1 are the wavelengths corresponding to the extinction coefficients σ_0 and σ_1,

200   respectively. Combining Eqs. (1), (6) and (7) yields an approximative MOR of

$$MOR \approx \frac{3}{\beta(\pi)S\left(\frac{\lambda_1}{\lambda_0}\right)^\alpha}, \qquad (8)$$

which is used to relate backscatter from the lidar to visibility. λ_0 and λ_1 are set to 1560 nm (Table 1) and 550 nm, respectively.

The two unknowns, α and S, depend on the aerosol type, and are a non-unique combination, which can be obtained by

matching the converted backscatter with the visibility from the in situ sensor. A typical value for α has been empirically

205   determined as 1.4 for visibilities between 6 and 20 km (Nebuloni et al., 2005), which is adopted here.

2.3.2 Method B: Fitting a transfer function

Coinciding visibility and backscatter data are selected and binned into 120 values of backscatter and 80 values of visibilities.

Figure 3 3 shows a scatter plot of the resulting distribution, representing a 2D-histogram, with the logarithm of the inverse

210   visibilities plotted against the logarithm of the lidar backscatter.

For the Cabauw visibility data, depending on the availability of both backscatter and visibility at a given height, and

depending on the height, there are between ~13000 and ~25000 samples, that is, coinciding visibility/backscatter pairs. There

appears to be a secondary mode (Figs. 3a and b), the origin of which is not entirely clear. A reasonable explanation could be a

contaminated visibility sensor window beyond the capability of the self-correcting algorithm of the visibility sensor, or it could

215   be residual cloud contribution. Visibilities greater than 20 km in the visiometer data were set to 20 km during acquisition,

which explains the disproportionally high accumulation of values at that visibility. Most of the data is concentrated below 20

km visibility, which therefore is deemed an appropriate upper range. It becomes clear from Figure 3a, that the data correlate

linearly only for a limited parameter range. Towards lower visibilities, the dependence becomes increasingly nonlinear. Only

visibilities of at least 4 km are considered, which helps to select a data range with reasonably linear correlation between

220   backscatter and inverse visibility and excludes the impact of fog or cloud on the visiometer readings.

For Pershore, visibility data from a single height only (2 m agl) were available. The nearest lidar data was for a

measurement range of 10 m agl, which was only available for a relatively short period, corresponding to only ~9000 coinciding

value pairs (samples). Therefore, lidar data from 39 m were chosen, associated with ~28000 coinciding samples (Fig. 3b). The

vertical separation is justified further below. There appear to be two modes: A correlation with relatively flat slope for high

225   visibilities, where data density is highest, and a steeper mode for visibilities below ~20 km. The nonlinearity of the visibility

with backscatter could be attributed to different contributions to the average aerosol size distribution (Curcio et al., 1958).

After binning, for each visibility, a threshold t is applied over the spectrum of backscatter values, which is computed as

$$t = \mu + \delta, \tag{9}$$

230 where μ is the mean sample density of the backscatter spectrum and δ is an adjustable parameter. The thresholding is used to exclude spectral outliers and artefacts (deemed to be unlikely values) and to tighten the distribution of backscatter values at given visibilities (reduce variance), corresponding to a forced reduction in samples. After thresholding, the first moment of the backscatter distribution (centroid) is retrieved for each of the 80 visibilities. This corresponds to a maximum likelihood estimation of the backscatter, i.e., the estimation of the expectation value of the distribution of backscatter-visibility sample.

235 The retrieved backscatter values for all 80 visibilities are then used for a linear fit, which also is a measure of linear correlation between visibility and lidar backscatter. The linear fit is then used as a transfer function (similar to a calibration) to translate a measured backscatter value from the wind lidar to visibility (or vice versa if desired).
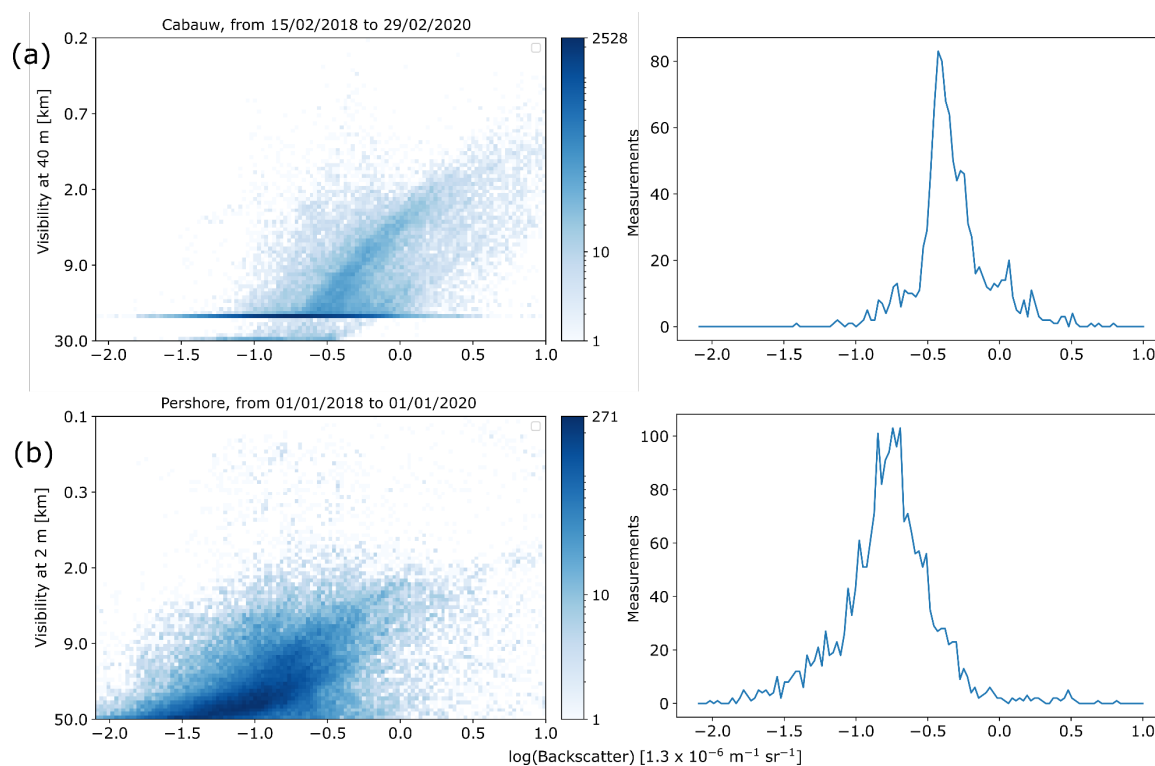
Figure 3. Overview correlation plots of inverse visibility versus backscatter (both logarithmised). For better readability, y-tick labels
240 **of visibility are shown. (a) For Cabauw, with backscatter distribution at 12 km visibility. Visibility measured at 40 m agl, backscatter from 39 m agl. (b) For Pershore, with backscatter distribution at 12 km visibility. Visibility measured at 2 m agl, backscatter from 39 m agl. The backscatter is logarithmic to facilitate display due to its large dynamic range.**

3. Results
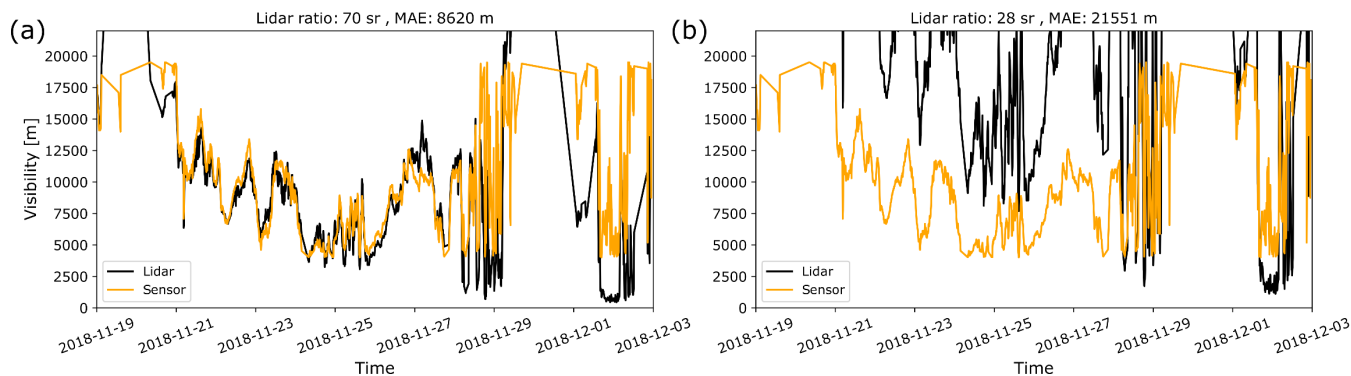
3.1 Method A

Figure 4. Linking backscatter from 39 m agl to visibility for Cabauw using Method A. (a) Lidar ratio is 70 (continental). (b) Lidar ratio is 28 (marine), the Ångström coefficient is 2.0 for both. The visibility sensor data are from 40 m agl.

Equation (8) is used to estimate visibility from wind lidar backscatter for Cabauw from the full visibility range (no selection or filtering is applied, see Fig. 3). The visibility estimate, Eq. (8), is very sensitive to the Ångström coefficient, whereas the choice of the lidar ratio is rather forgiving. The lidar ratio was held constant at 70 sr, representing a continental tropospheric SD (Jäger et al., 1995, Doherty et al., 1999). Changing the Ångström coefficient from the initial value of 1.4, which largely overestimated visibilities from the visiometer, to 2.0, associated with a finer, more continental aerosol dominating the backscatter, improved the fit considerably (Fig. 4a). The scatter of the data (Figs. 3a and b) translates into mismatches between the timeseries of backscatter and visibility. This does not explain why for some periods the visibilities match well (21/11 to 25/11/2018) and for some they do not (19/11, 29/11 to 3/12/2018). A more marine type lidar ratio of 28 sr (Doherty et al., 1999) associated with a larger aerosol mode size improves the fit somewhat for early December 2018, whilst largely overestimating the visibilities from the visibility sensor overall (Fig. 4b). The mean absolute error (MAE) for the whole period of 24 months of data is 8.6 km for a lidar ratio of 70, and over 21 km for a lidar ratio of 28, suggesting that the dominant aerosol at Cabauw is of continental type. The poor agreement for midday 19/11 and around 30/11 persists (Fig. 4a). This may partly be due to the visiometer data levelling off at 20 km visibility. The backscatter at midday of 19/11 was indeed ~4 times lower than during the morning of 19/11, hence with the same combination of $S = 70$ sr, $\alpha = 2$, thus leading to a fourfold increase in visibility (~58 km) as retrieved from the lidar backscatter. The aerosol SD and hence the Ångström coefficient and the lidar ratio usually vary over time, but in a confined manner (Doherty et al., 1999), thus leading to mismatches as in Fig. 4. The fitting would, therefore, need to be done daily. As demonstrate above, by varying the Ångström coefficient, a coarse fit could be produced, which could then be fine-tuned using the lidar ratio. Of course, this yields a nonunique solution. For example, $S = 28$ sr, $\alpha = 2.6$ yield a similar fit as in Fig. 4a, including MAE. Therefore, assumptions about the lidar ratio and Ångström coefficient would have to be made or lidar ratio and Ångström coefficient would need to be measured separately in parallel to lidar backscatter, such as with a nephelometer in combination with a sun photometer (Doherty et al., 1999). While

270 Method A is an interesting exercise, it is questionable whether it would be practical enough in obtaining a general transfer
function between lidar backscatter and visibility.

3.2 Method B

To that end method B was applied to the Cabauw data. A limited visibility range in the 2D-histogram of [4 km, 20 km] (Fig.
275 3a) was selected in order to increase linearity of the correlation. This was followed by thresholding using $\mu + 1.5$ (Fig. 5a).
After the thresholding is applied, the secondary mode has little influence on the fit, due to the relatively few points associated
with these backscatter/visibility pairs (Fig. 5b). The resulting histogram reveals a good correlation between visibilities from
the visibility sensor and the backscatter values from the wind lidar.

The lidar backscatter coefficient can be quite dynamic, changing by several factors within minutes. To assess whether
280 the 10 min averaging window caused any deterioration of the correlation, the time series were offset by up to 5 minutes before
averaging, with no significant effect on the correlation.

The ratio of the number of measurements with a given visibility versus the number of total measurements can be
computed to assess how frequent a given minimum visibility is. Using the visibility sensor data only, about 60% of the time,
visibility is at least 8 km (Fig. 5c). This may be compared with the fraction of measurements for a given visibility as retrieved
285 from the centroid backscatter values, which are in line, but slightly off, especially for the higher visibilities (68%, Fig. 5c).
This is caused by the slight nonlinearity in the correlation plot (Fig. 5a).

Method B was applied to the Pershore data set (Fig. 6a). Owing to the spread in backscatter, the R-squared value is
significantly lower than for Cabauw (0.80). The intercept for the Cabauw data is smaller than that for Pershore, whilst the
slope is slightly steeper, which indicates that the annual average backscatter is below that of Cabauw for all visibilities
290 considered here. This becomes easily visible when comparing the 1D- histograms (Figs. 5b and 6b). This implies that for the
same backscatter, the visibility at Pershore is smaller than at Cabauw. In line with the lower R-squared of the fit (Fig. 6a), the
discrepancy is higher between the prevalence of a given visibility for lidar derived versus sensor derived visibilities (Fig. 6c).
For example, a minimum visibility of 8 km was measured 62% of the time with the visiometer, but 82% of the time using lidar
derived visibilities from the transfer function. The closest agreement is for visibilities around 13 km, which is similar to
295 Cabauw (Fig. 5c).
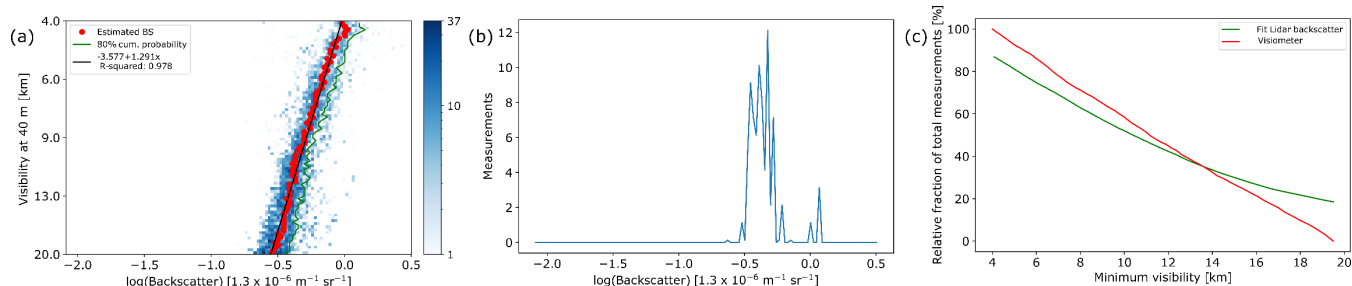
Figure 5. Visiometer readings versus lidar backscatter, for Cabauw. 39 m (40 m) agl for lidar (visiometer). Data covers full range from 13/07/2018 to 29/02/2020. (a) 2D-histogram. Overlain are the centroid BS (red dots), transfer function (black), 80% cumulative probability (green) for each visibility. (b) 1D slice at visibility of 12 km. (c) Relative fraction of total measurement for a given visibility using the fitted BS values and the visiometer data only.
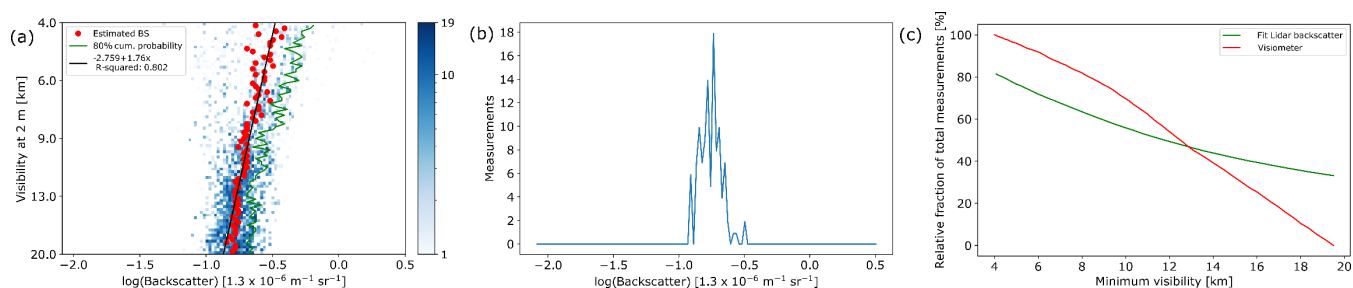
Figure 6. Visiometer readings versus lidar backscatter, for Pershore. 39 m (2 m) agl for lidar (visiometer). Data covers full range from 01/01/2018 to 01/01/2020. (a) 2D-histogram. Overlain are the centroid BS ((red dots), transfer function (black), 80% cumulative probability (green) for each visibility. (b) 1D slice at visibility of 12 km. (c) Relative fraction of total measurement for a given visibility using the fitted BS values and the visiometer data only.

3.2.1 Height dependence Cabauw

Only Cabauw data are considered since Pershore data was available for a single height only. While the correlation plots and the transfer functions for different heights of sensor and lidar do not reveal it directly (Fig. 7a to f), the visibilities computed from the fitted transfer functions of these correlations, show an upwards trend with increasing height (Fig. 8). It appears that visibility below ~80 m agl varies only little with height, which is in line with general observations of a vertically weakly exponential decrease in lidar signal strength (hence backscatter) that becomes significant above ~100 m agl. The temporal mean of the visibilities between 4 km and 19.5 km from the visiometers follow a similar trend (Fig. 8).

To assess the severity of separating visiometer height and lidar probe vertically, lidar backscatter from 39 m was correlated with visibilities from sensor heights not matching the lidar height. For the correlation of 39 m lidar vs. 200 m visiometer data, the difference in visibility to the visibility from the collocated sensor/lidar data (lidar at 39 m, visiometer at

315   40 m agl) is 35% (~3 km), with R-squared dropping to 0.81. Below that height, the difference is within 9% (800 m), that is, 1%, 9%, 3%, 3% with an R-Squared of 0.96, 0.97, 0.95, 0.89 for 10 m, 20 m, 80 m, 140 m, respectively. This is comparable to the relative change in visibility for heights up to 80 m agl. This indicates that, at least for this case, the visibility sensor and lidar probe height may be separated by few tens of metres, provided a generally well-mixed atmosphere within the layer, in which the sensor and lidar probe are located (as assumed for Pershore). This is also suggested by the time series of the visibility

320   sensors, which, for the heights of 10 m, 20 m, 40 m and 80 m agl largely correlate. Whilst this can be often be assumed for the continental boundary layer, especially during daytime, when convective mixing takes place, this would less likely to be expected offshore, for instance, due to the presence of advection fog near the sea surface, causing strong vertical gradients in aerosol density and SD.
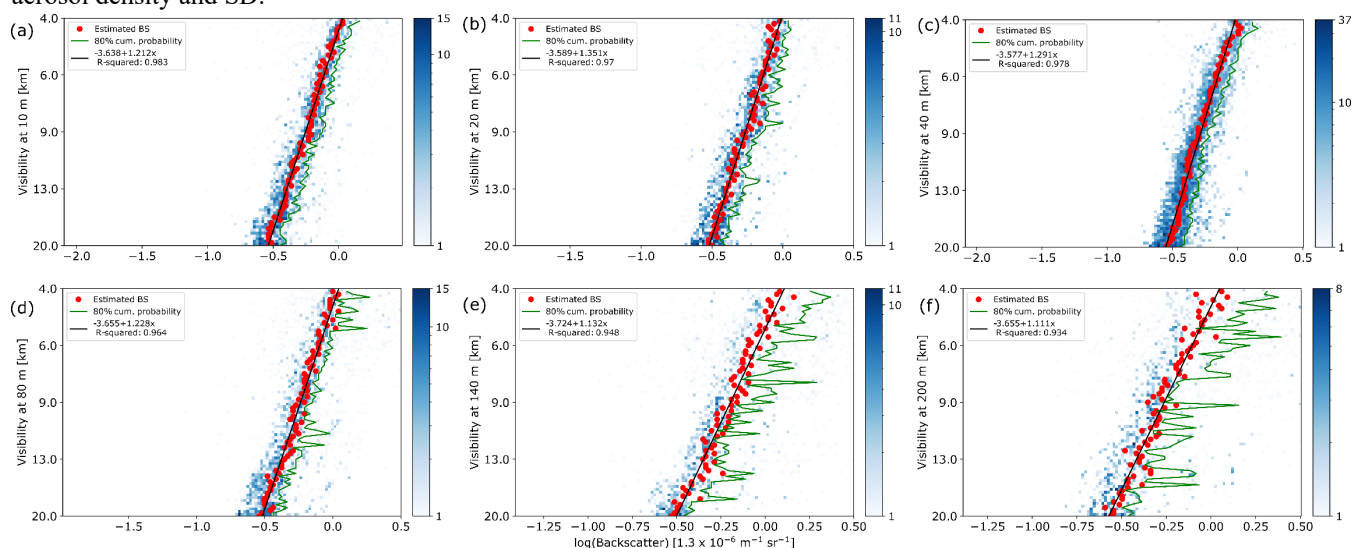
Figure 7. 2D-histograms for various measurement heights agl. (a) 10 m. (b) 20 m. (c) 40 m (d) 80 m. (e) 140 m. (f) 200 m above ground
325   **level. Overlain are: Centroid backscatter (red dots), transfer function (black), 80% cumulative probability (green) for each visibility**
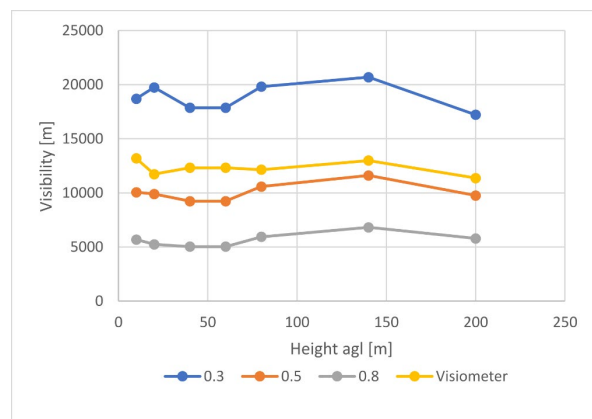
Figure 8. Visibility computed from all six transfer function (in Fig. 7) for three different backscatter values (in units of 1.3×10⁻⁶ m⁻¹
sr⁻¹) and temporal mean (15/2/2018 to 29/2/2020) of visiometer readings between visibilities of 4 km and 19.5 km as a function of
height.

330

3.2.2 Seasonality

Figure 9 shows 2D-histograms for 40 m agl, which underwent the same processing, as described in Method B, but split by seasons. The threshold has been lowered to $\mu + 1$ to partially compensate for the decrease in sample number which, if below ~4000, may deteriorate the linear correlation. The correlation still deteriorates for summer, due to fewer data points and a
335 larger scattering (only ~2500 data points vs ~8000 for other the seasons), especially for the less frequent lower visibilities. For Cabauw, the backscatter for all visibilities undergoes a strong shift to lower values from spring to summer to then remain relatively unchanged until autumn. Between autumn and winter, the backscatter mainly for the lower visibilities decreases, causing a decrease in slope of the transfer function. A backscatter of 0.4 (-0.4 in Fig. 9a) would give a visibility of ~13 km in spring, ~9 km during summer and winter and 8 km during autumn. For Pershore, the backscatter is distributed differently with
340 respect to visibility, but indicates a decrease from spring to summer and an increase from summer to autumn. A backscatter of 0.4 corresponds to visibilities of 2500 m, 1800 m, 4400 m, 1300 m (spring, summer, autumn, winter).

Reorganizing the backscatter data into monthly averages shows a clear seasonality for both Cabauw and Pershore (Fig. 10), which the 2D histograms do not reveal directly. As with the 2D-histograms, the monthly averages show a systematic difference in backscatter between the two sites that will be discussed further below. For both sites, the backscatter is highest
345 in the winter and lowest in the summer (Fig. 9). A backscatter minimum around July has been measured with different CW wind lidars in other locations in the Northern Hemisphere. Analysing monthly mean backscatter from Pershore for 9 years (2012 to 2020) resulted in a standard deviation of monthly mean backscatter over the years between 0.02 (July) and 0.09 (March). The z-score varied between 0.04 and 2.1. Depending on the year and month, the monthly mean backscatter, therefore, differed from the mean over 9 years by 0.04 to 2.1 standard deviations.
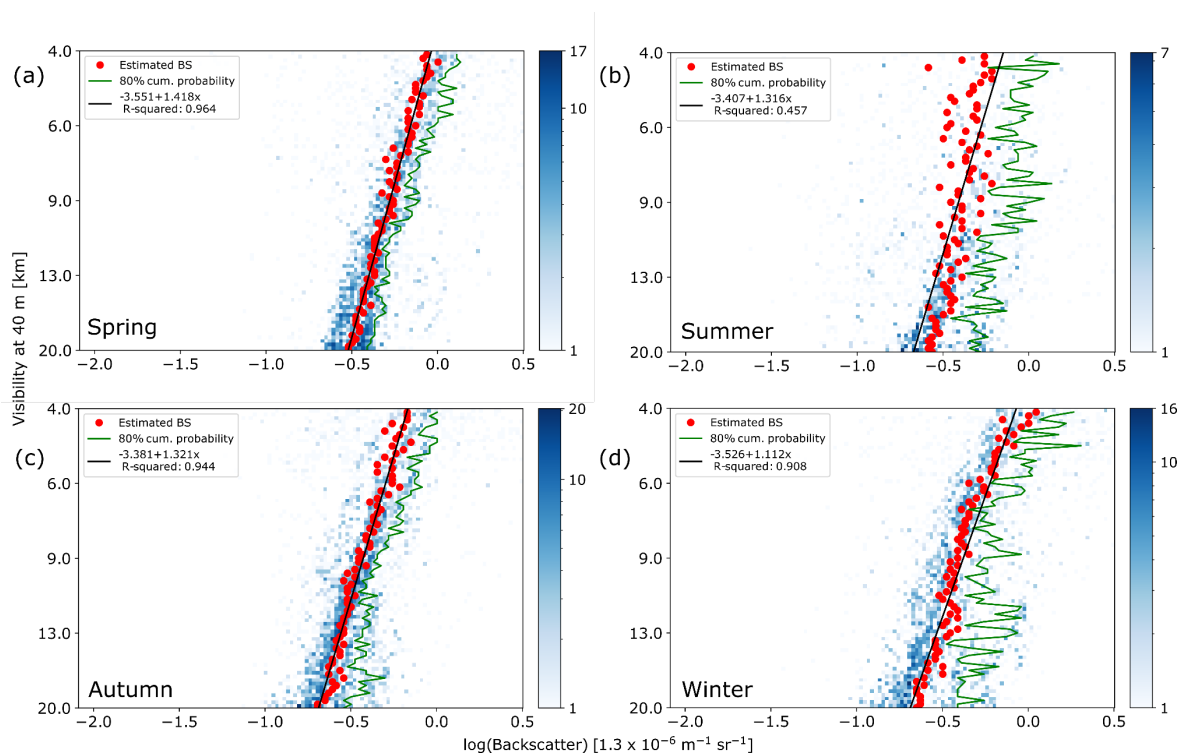
350

Figure 9. Cabauw data histograms split by seasons for visiometer height 40 m agl. (a) Spring. (b) Summer. (c) Autumn. (d) Winter.
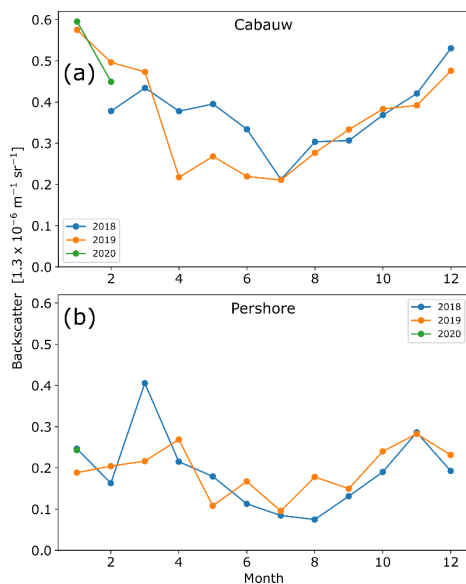
Figure 10. Monthly mean backscatter 39 m agl. (a) For Cabauw. (b) For Pershore.

3.2.3 Visibility time series

355   Figure 11 shows a visibility time series for Cabauw derived from lidar backscatter using the fitted transfer function (method B), covering the same period as Fig. 4 (method A). The lidar visibility was derived from lidar backscatter from 39 m agl against visibilities from the sensor at 40 m agl (Fig. 5). At places, the lidar derived visibilities agree well with visibilities from the visiometer (e.g. 21/11 to 26/11/2018), sometimes they largely disagree (e.g. 27/11), leading to an MAE of ~4 km for the whole 24 months covered by the data (an improvement over the MAE for method A, Fig. 4) and 2.1 km for the plotted period (Fig.

360   11a). The seasonality in the transfer function (Figs. 9 and 10) and the fact that the visiometer data are part of the fitting process, suggest that the closer the data acquisition period used for fitting the transfer function matches the period to predict visibilities, the better the agreement should become. Since the time series in Fig. 11 up to November corresponds to autumn, a reasonable period to choose data from should be autumn. When using data from autumn only to fit the transfer function, the MAE increases slightly from 2.1 km to 2.8 km, which is somewhat unexpected and will be investigated further below. The agreement around

365   27/11, however, improves (Fig. 11b). The MAE for the whole period of 24 months increased from ~4 km to ~5 km, as one would expect, since autumn only data were used to estimate visibility for all four seasons. When only data acquired in November are used for prediction (two months of data, 11/2018 and 11/2019), the agreement for the period displayed worsens (MAE 2.6 km), while the MAE for the whole 24 months remains at ~5 km (Fig. 11c). A very similar result is obtained, when data from November 2019 only are used to predict visibilities for the period displayed (Fig. 11d).

370   These tests do not support the hypothesis that the agreement between lidar derived visibilities and visiometer readings improves when the periods for fitting and predicting visibility match more closely. To assess that, other time periods underwent the same procedure with similar outcome. It was also found that limiting the data acquisition period has a similar effect as increasing the threshold. Regardless if spring, summer, autumn or winter is chosen, the overall MAE and the MAE of the period of interest decrease to comparable amounts (4 to 5 km and ~2 km, respectively). Limiting the data period further may

375   decreases the number of data and hence the goodness of the fit, at which point the MAE may increase. Increasing the threshold above a certain level may have the same effect. In practice, therefore, increasing the threshold of the fit has the same effect as limiting the data period for fitting (improves MAE), at least for the limited data set available here. For a very large data set (e.g. 10 years of data), however, matching the data period for the fit to that for the prediction could possibly be more beneficial than a simple thresholding of the 2D-histogram.

380   Decreasing the range of visibilities was also tested. It was found that MAE improved, at the cost of a lower dynamic range of visibilities in the time series, since the lidar derived visibility time series covers only visibilities that were used in the

fit of the transfer function. For instance, decreasing the range of visibilities to [7, 15] km led to a MAE of 1.6 km and 2.1 km, for the plotted period and the whole 24 months, respectively.
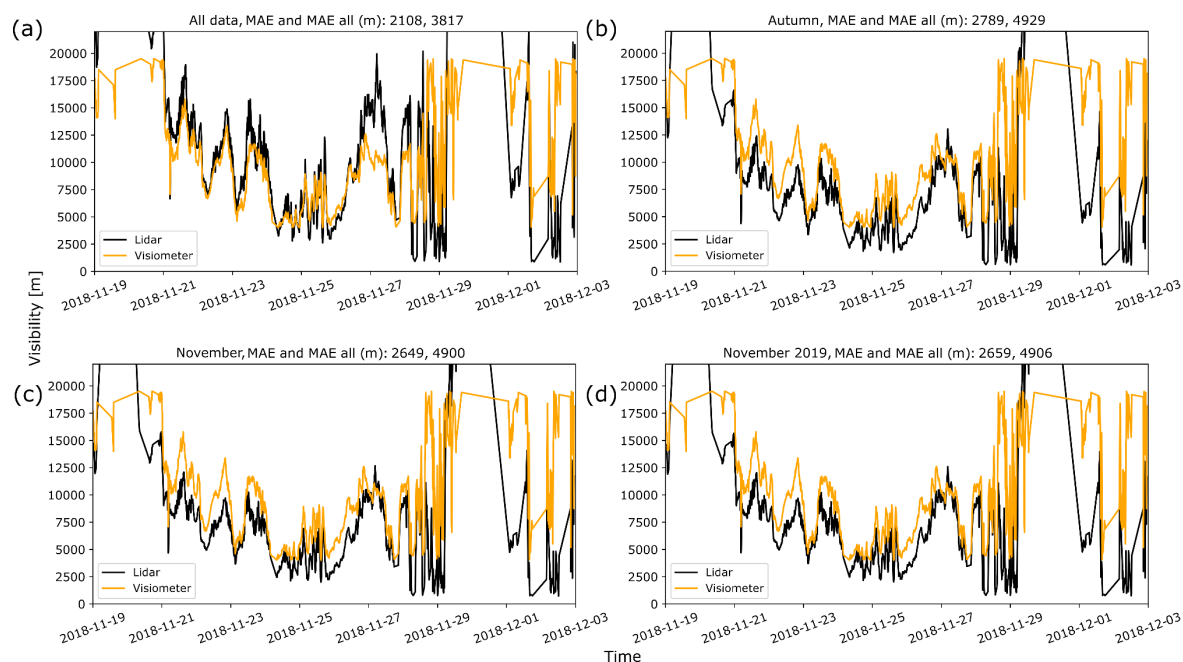
Figure 11. Lidar derived visibility time series and readings from visiometer for Cabauw. Also shown is the mean absolute error (MAE) between the two time series. MAE is for the plotted period only, MAE all is for whole data period of 24 months. (a) Fit used all data. (b) Fit used autumn data only. (c) Fit used data from Novembers only. (d) Fit used data from November 2019 only. Lidar derived visibilities outside the [4,20] km range used for retrieval have been excluded from the calculation of MAE, but are plotted to illustrate the effect of extrapolating the transfer function outside that range.

Figure 12 shows the visibility time series for Pershore, derived from lidar backscatter from 39 m agl against visiometer visibilities at 2 m agl (Fig. 6). Compared to Cabauw, the data for Pershore are less tightly clustered around the centroid backscatter values, especially for lower visibilities, which might be due to fewer data for these visibilities. Since the fit can approximately be interpreted as the visibility that corresponds to a given mean backscatter value with the width of the distribution indicating deviation, the larger spread of backscatter values leads to a correspondingly larger MAE between the time series of the lidar derived visibility and sensor visibility (Fig. 12). In other words, a given backscatter value corresponds to a larger range of visibilities. Increasing the threshold reduces the spread of the backscatter values at given visibilities (Figs. 6a and b) and, in fact, it reduces the MAE between the time series (Fig. 12a). An optimum threshold of $\mu + 1.5$ was found (Eq. (9)), which avoids deteriorating the linear fit (R-squared). As the threshold is increased, slope and intercept approach similar values as those for Cabauw. However, since the scale is logarithmic, even small differences lead to significant discrepancies in visibility and backscatter. The intercept visibility for Cabauw remains lower than for Pershore. For a given backscatter, and the visibility ranges regarded here, visibility remains smaller for Pershore than for Cabauw. A reduction in

MAE (overall MAE) from 3.8 km (4.8 km) to 3.5 km (4.4 km) is achieved when autumn data are selected (Figs. 12a and b). MAE remains unchanged for November data and decreases to 3.2 km (4.2 km) if only November 2019 data are used to predict visibilities.
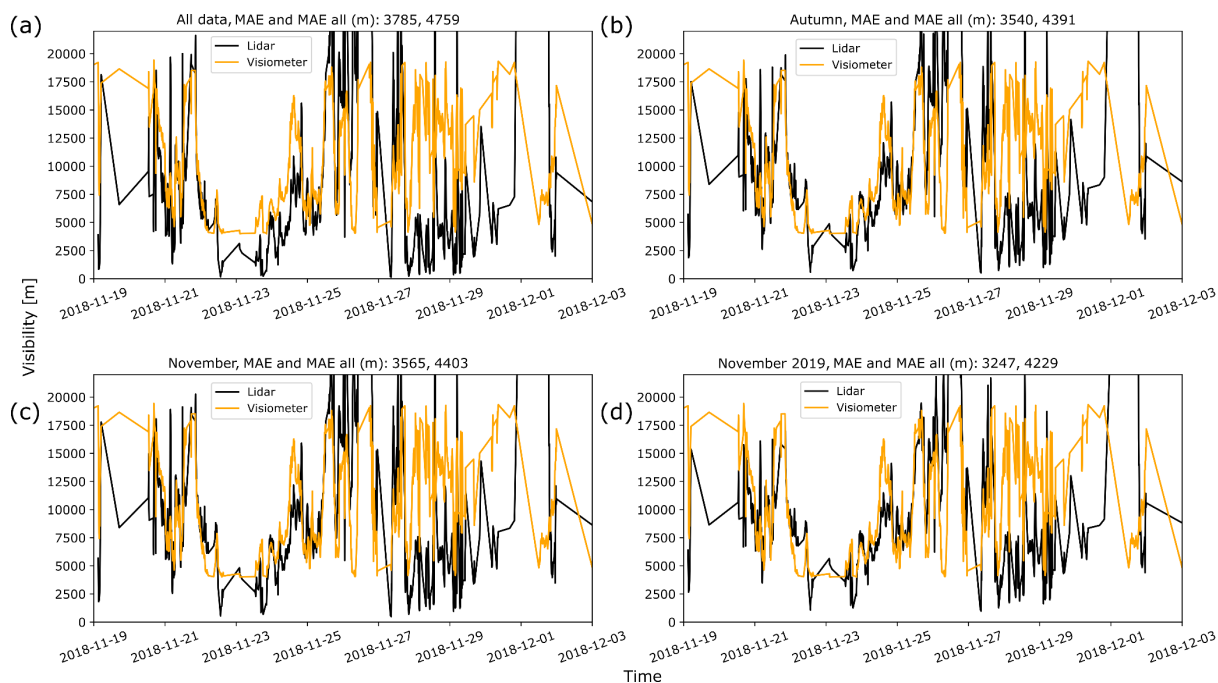
Figure 12. Lidar derived visibility time series and readings from visiometer for Pershore. Also shown is the mean absolute error (MAE) between the two time series. MAE is for the plotted period only, MAE all is for whole data period of 24 months. (a) Fit used all data. (b) Fit used autumn data only. (c) Fit used data from Novembers only. (d) Fit used data from November 2019 only. Lidar derived visibilities outside the [4,20] km range used for retrieval have been excluded from the calculation of MAE, but are plotted to illustrate the effect of extrapolating the transfer function outside that range.

4 Discussion

The backscatter values at a given visibility form a fairly mono-modal distribution. The transfer function is the linear least square fit of the first moments (centroids) of the distribution of backscatter values at given visibilities. It maps the most common backscatter value to visibility. The linear relationship between the centroids of the logarithmic backscatter and logarithmic inverse visibilities over a limited parameter range is in line with theory (Eq. (1)) and previous results (Curcio 1958; Twomey and Howell, 1965; Nebuloni, 2005). The smaller the range of visibilities considered, the more linear the relationship between logarithmic visibilities and backscatter, and hence the larger the R-squared value of the transfer function becomes. One would therefore expect that decreasing the visibility range would lead to enhanced agreement between sensor and lidar

420   derived visibilities, i.e., MAE decreases. While this is the case, it has little practical relevance, since the visibilities the transfer function would try to match were not included in the fit of the transfer function.

Assuming that the lidar backscatter probability density is monomodal, thresholding is applied to the distribution to remove artefacts and reduce the spread of the distribution at a given visibility. The transfer function changes after thresholding is applied. For example, for Cabauw the difference in visibility as a result of applying a threshold of $\mu + 0$ versus $\mu + 1$,

425   depending on the backscatter, amounts to a few hundred metres. Thresholding reduces data points and therefore may decrease the "goodness" of the linear fit, by increasing R-squared, which means the fit error variance (squared error) increases. One would expect this to ultimately cause an increase in MAE, since the fitted transfer function explains the data less well. On the other hand, the thresholding decreases the spread of backscatter values at a given visibility and decreases MAE with respect to visibilities from the visiometers, provided the number of data points is sufficient to form a mono-modal distribution (> 1

430   points around the centroid). The results, therefore, indicate that an optimum threshold exists that maximises R-squared, at the same time minimises MAE with reference measurements from the visiometers. In the present work this optimum has been roughly approached by trial and error, but certainly there is potential for an improved procedure.

The backscatter undergoes seasonal cycling and annual mean values of different years and monthly means between different years are reasonably comparable (Fig. 10). Since the monthly mean backscatter traces quite well the cycling in gross

435   primary productivity (Fleischer et al., 2015), it could be attributed to aerosol removal processes by leaved vegetation (Wedding et al., 1975). Other possible mechanisms include peaks in primary biological material (Held et al., 2008), a seasonality of condensed water aerosol in the planetary boundary layer and seasonal variations in boundary layer height, which influences dilution of aerosols.

Although both sites have the same qualitative seasonality in backscatter, when sorted by visibility in a 2D histogram

440   (Figs. 5 and 6), the trends are dissimilar, indicating that a given backscatter does not imply the same visibility at a different location. In fact, the backscatter at Pershore is systematically lower than at Cabauw. As mentioned above, differences between the visiometers should be insignificant. There is a contribution from the transmitted optical power of the wind lidars at the two sites. The transmitted power between units may vary by ~6%. Adding differences in receiver sensitivities between the two, the maximum expected difference in backscatter is of the order of 10%. As the observed differences are far greater than that, they

445   are in all likelihood related to the local aerosol properties, more specifically, to different dominant aerosol types. For instance, a visibility of 12 km corresponds to a backscatter of ~0.4 at Cabauw and ~0.18 at Pershore. Given that on a scale of minutes, the lidar backscatter value at a given site may easily vary by several factors, this difference is small. However, as it represents an average over many minutes, it is significant. Averaged on a monthly basis, the backscatter values at Cabauw are systematically greater than those for Pershore for each month of the year (Figs. 5 and 6). During the summer months, the

450   backscatter at Cabauw is about three times larger, during winter about two times larger than at Pershore (Figs. 9 and 10), suggesting differences in local atmospheric backscattering characteristics that may change with season. Interestingly, the backscatter values scatter considerably more around the expectation value for Pershore than for Cabauw. While we do not have an explanation for it, it also appears to be related to the site-specific average aerosol type.

These results are coherent with previous findings that reported a strong dependence of backscatter to the governing
455   aerosol mode (Twomey and Howell, 1964; Vogt 1968), as stated in the introduction of this paper. Although the extinction-to-
backscatter ratio (lidar ratio) is often assumed to be constant (including method A), this assumption is strictly speaking only a
fair approximation for homogenous scattering (such as Rayleigh scattering). As the size of the scattering particle increases,
Rayleigh scattering is replaced by the Mie scattering model, which, assuming spherical aerosols, is predominant for the present
study. Under Mie scattering, the assumption of isotropic scattering breaks down and the angular distribution of the scattered
460   electromagnetic field develops a directivity, i.e., an imbalance in the light intensities between forward scattering angles
(measured by visiometers) and the backscatter angle of π (measured by the wind lidar), which varies with size parameter $\alpha = 2\pi r / \lambda$ and therefore with particle radius r and wavelength λ (Vogt 1968, Shang et al., 2017). As the extinction-to-backscatter
ratio of a spherical particle changes with particle size, backscatter may vary strongly as particle type and size changes, even
along the beam, while the extinction coeffect varies only by a little bit (Tworney and Howell, 1965). The visiometers measure
465   forward scattering, and hence aerosol extinction, at angles with minimum sensitivity to changes in Mie-scattering intensity
upon change of particle type and size.

Since extinction and backscatter coefficients are quantities integrated over SD and size parameter, the fluctuation of
the lidar ratio (and hence backscatter) with particle size is smoothed. Real world aerosol SD are far from being homogeneous
and a smoothing effect can be expected. This also implies that the use of polychromatic light yields a backscatter intensity less
470   dependent on the aerosol SD than the highly monochromatic light of a coherent wind lidar. The result by Tworney and Howell
(1965) suggests that the use of monochromatic light contributes to the spread observed in the correlation between backscatter
and visibility with a factor of ~2, but it does not explain a systematic offset. The latter is more likely to be caused by a different
local aerosol SD to which the backscatter is more sensitive than forward scatter at the angular ranges used in the visibility
sensors.

475   With the abovesaid, it appears likely that different aerosol types (or SDs) may give a similar forward scattering
intensity, hence similar visibility sensor reading, but different backscatter values. Different sites are associated with a different
predominant (mean) aerosol SD, which, therefore, qualitatively could explain not only the variance (spread) of the lidar
backscatter value for a given visibility (e.g. Fig. 6a), but also the offset by a factor of 2 to 3 between the two distributions of
the two sites (Fig. 6). Of course, since aerosol density affects backscatter, a mean aerosol number density systematically lower
480   throughout the year would certainly contribute to the observed offset. Since the difference in transfer function is in all
likelihood related to differences in the predominant, local aerosol SD and/or particle number density, this indicates that after
calibrating the backscatter measured by the CW wind lidar (method B), the lidar could be used to measure visibility. The same
applies to method A.

Since the predominant aerosol SD in the planetary boundary layer is a function of location and the transfer function
485   has been found to vary between different locations, the transfer function is probably not generalizable, but site specific. Even
if the transfer function was similar for aerosol SD typical to a certain setting (e.g. marine, near coastal), it would not necessarily

be transferrable to a different location, since the local aerosol SD could become atypical, for instance, if the location is near a heavy polluter, such as a dense urban area.

The more it is known about the dominant aerosol probed by the lidar the more the transfer function could potentially
490   be applied to different locations with similar average aerosol SDs. It is therefore desirable to gain more information on the predominant aerosol type at Pershore and Cabauw. This would require a different set of instruments, which is beyond the scope of this work. Pershore is located in a rural area. During the predominant south-westerly and westerly winds, air coming from the Atlantic Ocean passes a strip of land about 300 km wide before it reaches Pershore. This area lacks major industry hubs or urban areas that would concentrate sea or road traffic and act as strong polluters. The dominant aerosol SD is thus likely a rural
495   one, which might be disturbed by road traffic. This is indicated by a pronounced difference in the transfer function fitted on weekend and weekday data and which could also be confirmed by observation.

During the predominant south-westerly winds, the aerosol type and number density around Cabauw is expected to be heavily influenced by road traffic aerosol from the Rotterdam suburban area, including the sea port (Karl et al., 2016), and remnants of combustion aerosol from the southeast of England, notably the London area (Fig. 2a). The strong concentration
500   of aerosols from both road and sea traffic and industrial air pollution downwind of Rotterdam and Rotterdam harbour may explain the larger average backscatter at Cabauw and hence the difference in intercept of the transfer functions between the two sites. The difference in slope, on the other hand, is likely dominated by the difference in the lidar ratio, i.e., it is due to different dominating aerosol type(s) at the two sites.

Splitting the data into day and night may also yield hints as to which extent man-made aerosols are dominating.
505   However, other diurnal mechanisms most certainly will affect aerosol type and number density, and hence lidar backscatter, such as meteorological processes, for example boundary layer mixing processes (Stanier et al., 2004). Interestingly, for Cabauw (Figs. 13a and b) the backscatter significantly increases during the night (18:00 to 6:00) for both 19 km visibility (by ~40%, from 0.215 to 0.290) and 5000 m visibility (by ~20%, from 0.673 to 0.808). A backscatter of 0.5 (-0.3 in Fig. 13) would give a visibility of ~7.1 km for the day fit and ~9.5 km if considering night time data only. For Pershore (Figs. 13c and d), no
510   significant change in backscatter was found during night time for 19 km visibility, but a pronounced decrease for 5 km visibility of 20% (from 0.328 to 0.261). Though not adequate to indicate man-made aerosol, splitting the data into day and night is insightful as it further demonstrates the sensitivity of linking visibility to lidar backscatter. For practical application that target daylight visibility, it may be advisable to exclude night-time data before fitting the transfer function.
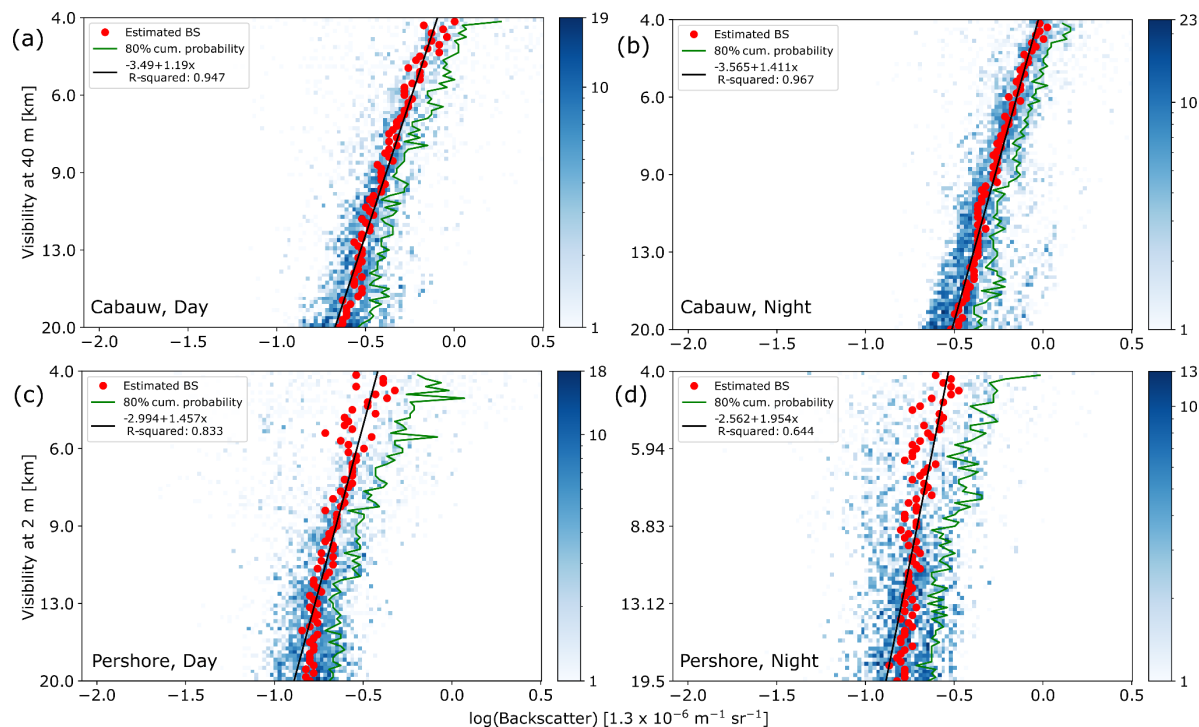
515

Figure 13. Comparison of 2D-histograms between day and night time at 39 m lidar probe height (a) Cabauw day. (b) Cabauw, night. (c) Pershore, day. (d) Pershore, night. To account for the reduced sample size, the threshold was reduced to $\mu + 1$.

In the Mie-scattering regime, which assumes spherical particles, the polarisation of light is preserved. The polarisation transmitted by the wind lidar is random and the polarisation of transmitted and received photons is assumed to be equal.

520 Depolarization effects by aerosols could, however, influence backscatter intensity. The technique used by the visiometers, on the other hand, is polarization insensitive. Two aerosol types, spherical (e.g. water droplets) and non-spherical (e.g. sea salt aerosols), may thus cause similar scattering intensities, but due to a change in polarization (depolarisation) caused by the non-sperical aerosol, the backscatter as detected by the wind lidar may differ, which will contribute to a site-specific transfer function.

525 For Cabauw, lidar backscatter derived visibility was found to be height dependent (Fig. 8), in line with the observation that under cloud free conditions backscatter from CW-wind lidar usually tends to slightly decrease with height in the lower part of the planetary boundary layer. The coherence of vertical trends of visibility as seen between wind lidar and the visiometer and lidar is encouraging in that it suggests that once calibrated, a CW wind lidar may indeed be useful in generating profiles of SOR in situations where visiometers at heights above tens of m agl are not available or feasible.

530

Conclusions

Backscatter data from two CW-wind lidar systems, one at Cabauw (Netherlands) and one at Pershore (UK) have been analysed with the aim to retrieve meteorological optical range (visibility). Directly relating backscatter to visibilities was found less practical due to the need for additional input parameters. Correlating lidar backscatter coefficients with co-measured visibilities from visiometers and fitting a linear transfer function to points of maximum likelihood backscatter was found to be more

535 viable, as it would not rely on secondary measurements acquired in parallel.

For larger ranges of visibility and backscatter coefficients, the correlation was found to be less linear, which means the method deems practical only over a limited parameter range. This can be explained by different aerosol types and size distributions at play for different backscatter coefficients. Furthermore, differences in local dominant aerosol type lead to

540 differences in extinction-to-backscatter ratio between the two sites and thus differences in the transfer function. In other words, two different aerosol types may give a similar forward scattering intensity, hence similar visibility sensor reading, but a different backscatter and thus a different wind lidar-derived visibility. Therefore, backscatter measurements from CW wind lidar are only representative and repeatable for environments with similar aerosol SDs. More long-term tests are needed to assess to which extend the calibration needs to be repeated or if it needs to be repeated if the location is kept fixed.

545 In line with previous findings, the result suggests that backscatter from CW-wind lidar is useful to infer visibility, but it needs to be calibrated against a visibility sensor in an atmosphere similar (similar mean aerosol type) to the one of its intended use, ideally over the course of a year to capture seasonal variation. It may also be helpful in the future to confirm or refine this conclusion by measuring at more sites globally and categorize them into sites with similar predominant mean aerosol SD. Getting visibility data from more sites is desirable to test how site specific the transfer function is and how comparable it is

550 between similar environmental settings. As far as the two sites assessed in this study are concerned, even after calibrating the lidar backscatter with an in-situ visibility sensor at the site of intended use, the expected accuracy in terms of mean absolute error is over a kilometre. The method would thus deem suitable only for safety uncritical applications, such as industrial (e.g. visibility of wind turbines, oil rigs from the shore etc.) or in scientific research. A possible application could include the statistical estimation of the frequency of wind turbines visibility. This could especially be interesting for offshore sites, where,

555 for economic reasons, the distance between the windfarm and the shore has to be minimized. The MOR derived from backscatter could be one of several input parameters amongst other parameters, such as solar angle, object colour, Earth's curvature, or cloud cover. Since the backscatter depends critically on the aerosol SD, this could potentially open up applications where sensitivity to aerosol chemistry is desired, such as pollution monitoring or detecting changes in particular matter properties during passive and eruptive degassing phases of volcanoes, which are linked to physiochemical processes inside the

560 volcanoes' plumbing systems.

Data availability

Cabauw tower and surface data sets are available as: Meteo profiles - validated tower profiles of wind, dew point, temperature and visibility at 10 minute interval from https://dataplatform.knmi.nl/dataset/cesar-tower-meteo-lb1-t10-v1-2 and Meteo
565   surface - validated observations of common atmospheric variables at 10 minute interval from https://dataplatform.knmi.nl/dataset/cesar-surface-meteo-lb1-t10-v1-0. Pershore visibility data are available at https://zenodo.org/record/6325902#.YiDrNejP2Uk (Queißer et al., 2022). Backscatter data is available from the first and second author on request.

Author contributions

570   SK was responsible for the wind lidar measurement campaign at Cabauw. MQ and MH performed the data analysis and wrote the draft. All authors worked on the refinement of the manuscript.

Competing interests

The authors declare that they have no conflict of interest.

575   **Acknowledgements**

We thank Matt Smith and Scott Wylie (both ZX Lidars) for the inspiration for this paper and helpful discussions.

References

580   Bi, L., Lin, W., Wang, Z., Tang, X., Zhang, X., and Yi, B.: Optical modeling of sea salt aerosols: The effects of nonsphericity and inhomogeneity. J. Geophy. Res. Atmos., 123, 543-558., doi: 10.1002/2017JD027869, 2018.

Biral SWS Series user manual, available at: https://www.biral.com/wp-content/uploads/2018/02/SWS-Manual-105223.08B.pdf (last accessed 2/3/2022), 2018.
585

Bosveld, F. C.: The Cabauw In-situ Observational Program 2000 - Present: Instruments, Calibrations and Set-up, KNMI, Technical Report, TR-384, available at: https://cdn.knmi.nl/knmi/pdf/bibliotheek/knmipubTR/TR384.pdf (last accessed 29/3/2022), 2020.

590

Button, J. L. and Iyer, R. S.: Continuous wave lidar measurement of atmospheric visibility, Appl. Opt., 17, 265, doi:10.1364/ao.17.000265, 1978.

Crosby, J. D.: Visibility sensor accuracy: what's realistic, in: 12th Sympsium on Meterological Observations and Instrumentation, Long
595   Beach, CA, USA, 9-13, 2003.

Cambell Scientific CS125 user manual, available at: https://s.campbellsci.com/documents/ca/manuals/cs120a-cs125_man.pdf (last accessed 2/3/2022), 2016.

600   Curcio, J. A. and Knestrick, G. L.: Correlation of Atmospheric Transmission with Backscattering, J. Opt. Soc. Am., 48, 686, doi:10.1364/josa.48.000686, 1958.

Dabberdt, W. F. and Eigsti, S. L.: Regional visibility modeling for the Eastern United States. Atmos. Environ., 15, 2055–2061, doi:10.1016/0004-6981(81)90238-9, 1981.
605

Emeis, S., Harris, M., and Banta, R. M.: Boundary-layer anemometry by optical remote sensing for wind energy applications, Meteorol. Z., 16, 337-347, doi:10.1127/0941-2948/2007/0225, 2007.

Fernald, F., B. Herman, and J. Reagan: Determination of aerosol height distributions by lidar, J. Appl. Meteor., 11, 482-489,
610   doi:10.1175/1520-0450(1972)011<0482:DOAHDB>2.0.CO;2, 1972.

Fleischer, K., Warlind, D., Van der Molen, M., Rebel, K. T., Arneth, A., Erisman, J. W., Wassen, M., Smith, B., Gough, C., Margolis, H., Cescatti, A., Montagnani, L., Arain, A., and Dolman, A. J.: Low historical nitrogen deposition effect on carbon sequestration in the boreal zone, J. Geophys. Res. Biogeosci., 120, doi:10.1002/2015JG002988, 2015.
615

Gerber, H.: Relative - Humidity Parameterization of the Navy Aerosol Model (NAM)., NRL Report 8956, Naval Research Laboratory, Washington, DC, 1985.

Hänel, G.: The Single-Scattering Albedo of Atmospheric Aerosol Particles as a Function of Relative Humidity, J. Atmos. Sci.,
620   33, 1120 -1124.

Harris, M., Constant, G., and Ward, C.: Continuous-wave bistatic laser Doppler wind sensor. Appl. Opt. 40, 1501-1506, 2001.

Held, Andreas, Zerrath, A., McKeon, U., Fehrenbach, T., Niessner, R., Plass-Dülmer, C., Kaminski, U., Berresheim, Harald, and Pöschl, U.: Aerosol size distributions measured in urban, rural and high-alpine air with an electrical low pressure impactor (ELPI), Atmos. Env., 42, 8502-8512, doi:10.1016/j.atmosenv.2008.06.015, 2008.

Hongda T., Xiaohua, K., Zibo, Z., and Dongsong, S.: Performance of backscatter visibility lidar at UYN airport. Selected Papers of the Chinese Society for Optical Engineering Conferences, doi:10.1117/12.2264816, 2016.

Hu, L., and Hao Yang, H.: Monitoring and analysis of sea fog in an offshore waterway using lidar, Opt. Eng., 60, 064103, doi:10.1117/1.OE.60.6.064103, 2021.

Jäger, H., Deshler, T., and Hofmann, D. J.: Midlatitude lidar backscatter conversions based on balloonborne aerosol measurements, Geophys. Res. Lett., 22, 1729-1732, doi:10.1029/95gl01521, 1995.

Jones, D.W., Ouldridge, M., and Sparks, W. R.: The first WMO intercomparison of visibility measurements: final report, published by WMO, available at: https://library.wmo.int/index.php?lvl=notice_display&id=11248#.Yh99aejP2Uk (last accessed: 2/3/2022), 1990.

van Jaarsveld, J. A., and Klimov, D.: Modelling the impact of sea-salt particles on the exceedances of daily PM10 air quality standards in the Netherlands, Int. J. Environ. Pollut., 44, 217–225, 2011.

Karl, M., Kukkonen, J., Keuken, M. P., Lützenkirchen, S., Pirjola, L., and Hussein, T.: Modeling and measurements of urban aerosol processes on the neighborhood scale in Rotterdam, Oslo and Helsinki, Atmos. Chem. Phys., 16, 4817-4835, doi:10.5194/acp-16-4817-2016, 2016.

Knoop, S., Bosveld, F. C., de Haij, M. J., and Apituley, A.: A 2-year intercomparison of continuous-wave focusing wind lidar and tall mast wind measurements at Cabauw, Atmos. Meas. Tech., 14, 2219–2235, https://doi.org/10.5194/amt-14-2219-2021, 2021.

Kreid, D. K.: Atmospheric visibility measurement by a modulated cw lidar, Appl. Opt., 15, 1823. doi:10.1364/ao.15.001823, 1976.

Middleton, W. E. K.: Visibility in Meteorology: The Theory and Practice of the Measurement of the Visual Range. University of Toronto Press, Toronto, Canada, 1947.

Nebuloni, R.: Empirical relationships between extinction coefficient and visibility in fog, Appl. Opt., 44, 3795-3804, doi:10.1364/ao.44.003795, 2005.

Pantazis, A., Papayannis, A., Georgousis, G.: Lidar algorithms for atmospheric slant range visibility, meteorological conditions detection, and atmospheric layering measurements, Appl. Opt., 56, 6440-6449, 2017.

Queißer, M., Harris, M., and Knoop, S.: Atmospheric visibility inferred from continuous-wave Doppler wind lidar, data set Data set, Zenodo, https://doi.org/10.5281/zenodo.6325902, 2022.

Shang, X., Xia, H., Dou, X., Shangguan, M., Li, M., Wang, C., Qiu, J., Zhao, L., Lin, S.: (2017). Adaptive inversion algorithm for 1.5 um visibility lidar incorporating in situ Angstrom wavelength exponent, Opt. Comm., 418, doi: 10.1016/j.optcom.2018.03.009, 2017.

Schappert, G. T.: Technique for Measuring Visibility, Appl. Opt., 10, 2325, doi:10.1364/ao.10.002325, 1971.

Schuster, G. L., Dubovik, O., and Holben, B. N.: Angstrom exponent and bimodal aerosol size distributions, J. Geophys. Res.: Atmos., 111, doi: https://doi.org/10.1029/2005JD006328, 2006.

Smith, D. A., Harris, M., Coffey, A. S., Mikkelsen, T., Jørgensen, H. E., Mann, J., and Danielian, R.: Wind lidar evaluation at the Danish wind test site in Høvsøre, Wind Energy, 9, 87-93, https://doi.org/10.1002/we.193, 2006.

Stanier, C. O., Khlystov, A. Y., and Pandis, S. N.: Ambient aerosol size distributions and number concentrations measured during the Pittsburgh Air Quality Study (PAQS). Atmos. Environ., 38, 3275-3284, doi:10.1016/j.atmosenv.2004.03.02, 2004.

Twomey, S. and Howell, H. B.: The Relative Merit of White and Monochromatic Light for the Determination of Visibility by Backscattering Measurements, Appl. Opt. 4, 501-506, 1965.

Vogt, H.: Visibility Measurement Using Backscattered Light, J. Atmos. Sci., 25, 912-91, doi:10.1175/1520-0469(1968)025<0912:VMUBL>2.0.CO;2, 1968.

Wedding, J. B., Carlson, R. W., Stukel, J. J., and Bazzaz, F. A.: Aerosol deposition on plant leaves. Environ. Sci. Technol.,
690   9, 151-153, doi:10.1021/es60100a004, 1975.

Wiedensohler, A., Wehner, B., and Birmili, W.: Aerosol Number Concentrations and SDs at Mountain-Rural, Urban-Influenced Rural, and Urban-Background Sites in Germany, J. Aerosol Med., 15, 237-243, doi:10.1089/089426802320282365, 2002.

695

Winker, D. M., Tackett, J. L., Getzewich, B. J., Liu, Z., Vaughan, M. A., and Rogers, R. R.: The global 3-D distribution of tropospheric aerosols as characterized by CALIOP, Atmos. Chem. Phys., 13, 3345-3361, doi:10.5194/acp-13-3345-2013, 2013.

700   Werner C., Streicher J., Leike I., Münkel C.: Visibility and Cloud Lidar, in: Weitkamp C. (eds) Lidar. Springer Series in Optical Sciences, 102, Springer, New York, NY, doi:10.1007/0-387-25101-4_6, 2005.

Young, S. A., Vaughan, M. A., The Retrieval of Profiles of Particulate Extinction from Cloud-Aerosol Lidar Infrared Pathfinder Satellite Observations (CALIPSO) Data: Algorithm Description, J. Atmos. Ocean. Technol., 26, 1105-705   1119, doi:10.1175/2008jtecha1221.1, 2009.

Yu, Q.-R., Zhang, F., Li, J., and Zhang, J.: Analysis of sea-salt aerosol size distributions in radiative transfer, J. Aeros. Sci., 129, 71-86, doi:10.1016/j.jaerosci.2018.11.01, 2018.